

IMECE2010-38767

COMPUTATIONAL STUDY OF THE SYNTHETIC JET ON SEPARATED FLOW OVER A BACKWARD-FACING STEP

Koichi Okada

Department of Ocean and
Space Engineering, Yokohama
National University
Yokohama, Kanagawa, Japan

Akira Oyama

JAXA/Institute of Space and
Aeronautical Science
Sagamihara, Kanagawa, Japan

Kozo Fujii

JAXA/Institute of Space and
Aeronautical Science
Sagamihara, Kanagawa, Japan

Taku Nonomura

JAXA/Institute of Space and
Aeronautical Science
Sagamihara, Kanagawa, Japan

Koji Miyaji

Department of Ocean and Space
Engineering, Yokohama National
University
Yokohama, Kanagawa, Japan

Kengo Asada

Department of Aeronautics and
Astronautics, University of
Tokyo
Sagamihara, Kanagawa, Japan

ABSTRACT

Frequency effects of the synthetic jet on the flow field over a backward facing step are investigated using numerical analysis. Three-dimensional Navier-Stokes equations are solved. Implicit large-eddy simulation using high-order compact difference scheme is conducted. The present analysis is addressed on the frequency characteristics of the synthetic jet for understanding frequency characteristics and flow field. Three cases are analyzed; the case computing flow over backward facing step without control, the case computing flow with synthetic jet control at $F_h^+ = 0.2$, and the case computing flow with synthetic jet control at $F_h^+ = 2.0$, where non-dimensional frequency F_h^+ is normalized with the height of backward-facing step and the freestream velocity. The present computation shows that separation length in the case of the flow controlled at $F_h^+ = 0.2$ is 20 percent shorter than the case without control. Strong two-dimensional vortices generated from the synthetic jet interact with the shear layer, which results in the increase of the Reynolds stress in the shear layer region. These vortices are deformed into three-dimensional structures, which make Reynolds stress stronger in the recirculation region. Size of the separation length in the case of the flow controlled at $F_h^+ = 2.0$ is almost the same as the case without control because the mixing between the synthetic jet and the shear layer is not enhanced. Weak and short periodic vortices induced from the synthetic jet do not interact with the shear layer very much and diffuse in the recirculation region.

INTRODUCTION

Recently, active flow control using microscale devices has received increasing attention. A type of such flow control devices is a "synthetic jet," which consists of an orifice connected to a cavity, the bottom which oscillates with a small amplitude and produces weak and periodic flow from the orifice (Fig. 1). A study in the literature reported that flow separation over a wing can be controlled by a synthetic jet inducing weak and periodic flow from its orifice exit.[2,3] An advantage of using synthetic jets over conventional flow control devices is their active flow-control capability, because the induced flow can be controlled electrically. Another advantage of synthetic jets is their light weight and compactness, as they do not require any pneumatic supply. Due to these advantages, synthetic jets are considered suitable for various aircrafts, especially for unmanned air vehicles, microscale air vehicles, and rotorcraft.

Most of previous experimental studies on the synthetic jet have been focused on demonstrating effects of the synthetic jet for flow control, or finding optimal conditions for the synthetic jet on an airfoil or backward facing step. In experimental studies, Amitay *et al.* [3] and Seifert and Darabi [4] parametrically studied in their experiments the effects of the position of installation, non-dimensional jet frequency (based on chord length or separation length and free stream velocity), and the jet mass flow on the flow separation control around an

airfoil. Glezer *et al.* [5] researched especially non-dimensional jet frequency effects on the flow separation control around an airfoil. Previous research [4] showed that actuation with nondimensional jet frequency of $O(1)$ works well, but they showed that actuation with nondimensional jet frequency of $O(10)$ works much better. On the other hand, Yoshioka *et al.* [6] studied experimentally separation control of backward-facing step configuration using periodic excitation and showed that actuation with nondimensional frequency F^+_h (based on height of backward-facing step and freestream velocity) of 0.2 works better. However, the flow control mechanism of the synthetic jet has not been clear yet.

To date, the application of synthetic jets has been limited to the control of low-speed flows, because the output power of synthetic jets is relatively small. Therefore, to make synthetic jets applicable for high-speed flow control, it is necessary to understand the flow control mechanism of synthetic jets and re-design it by using a physics-based model instead of current trial-and-error experimental studies. The technology of separation flow control using the synthetic jet of actual aircraft level (High Reynolds number, high dynamics pressure, large scale) has not been developed, yet.

Thus far, the characteristics of synthetic jet themselves have not been well-discussed including fine vortex structure inside cavity. Therefore, in the previous study [7], three-dimensional flow inside the synthetic jet cavity and orifice and the flow outside the cavity are simulated together using large-eddy simulations (LES) as first step. Firstly, the computation of synthetic jet blowing to static air was conducted and effects of synthetic jet parameters on the induced flow field were investigated. Comparison of the present LES result with experimental data showed that three-dimensional modeling of the flow inside the cavity is essential for accurate estimation of the velocity and velocity fluctuations of the synthetic jet. This indicates that the three-dimensional vortex structure created inside the cavity probably plays an important role in flow control with a synthetic jet. Comparison of the present LES results for different Reynolds number flow conditions showed that there is a significant difference in the damping rate of the velocity fluctuations, while no remarkable difference is observed in the damping rate of the time-averaged vertical velocities. Comparison of the present LES results for different Strouhal number flow conditions showed that finer vortex structure is formed and the time-averaged velocity and velocity fluctuations diffuse faster for high Strouhal numbers. From the results, parameters effects of the synthetic jet itself were well clarified.

Now, we analyze the flow-fields of the synthetic jet for separation-flow control to understand the mechanics of separation-flow control using the synthetic jet as second step. In order to understand the mechanism of the synthetic jet on the massively separated flow which appears at the backward-facing step for design of the synthetic jet, flow-fields with/without the synthetic jet are numerically simulated. A backward-facing step configuration is chosen for this research because the flow field

and geometry become simpler than those around an airfoil and there are a few flow condition parameters. Many previous studies showed frequency effect for separation control and there are two different opinions of frequencies ($F^+=1$ and $F^+=10$) for separation control. Thus, the present analysis is focused on the frequency characteristics of the synthetic jet controlling separated flow.

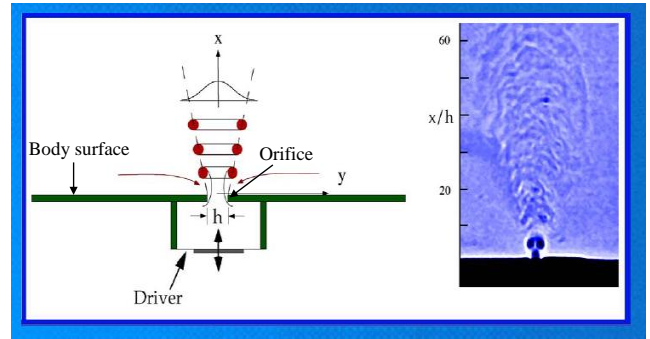


Fig. 1. Synthetic jet [2]

NOMENCLATURE

A	=	amplitude of the wall oscillation
$C\mu$	=	Non-dimensional momentum ratio
d	=	width of synthetic jet orifice
f	=	Dimensional frequency of synthetic jet
F^+_h	=	Non-dimensional frequency of synthetic jet
h	=	height of backward-facing step
M_∞	=	free stream Mach number
ρ	=	free stream density
Re_h	=	Reynolds number based on h
t	=	Non-dimensional time
u_{jet}	=	averaged maximum velocity at orifice exit
u_∞	=	free stream velocity
X_L	=	cavity width
Z_D	=	cavity depth

COMPUTATIONAL CONDITIONS

A. Configuration of synthetic jet

A geometric configuration of the synthetic jet in the reference [15] is chosen in this study (Fig. 2). The non-dimensional orifice depth d is equal to the non-dimensional orifice width h . The cavity depth Z_D is $10d$ and the cavity width X_L is $15d$. The cavity span length in the y direction is treated to have infinite length in the simulation since this study target two-dimensional configuration.

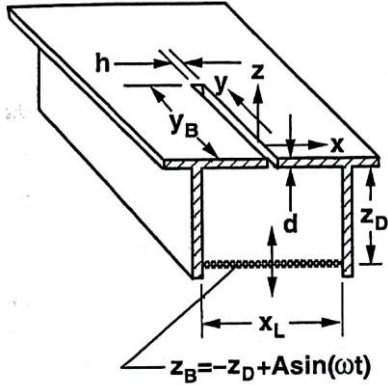


Fig. 2. Synthetic jet configuration [15]

The oscillation of the cavity wall is defined by equation (1).

$$h_w(x, t) = A \cdot \sin(2\pi F_h^+ t) \quad (1)$$

Here, amplitude of the wall oscillation A is constant value. F_h^+ is non-dimensional frequency of the wall oscillation. Input parameters are shown in the section of flow conditions.

B. Configuration of Backward-facing step

The backward-facing step configuration and flow conditions are same of Jovic's study [17] because this experiment has various comparable data for validation of the case without synthetic jet control. Figure 3 shows the backward-facing step configuration. All scales in figure are in centimeter; but the figure is not in scale. A part colored by cyan shows computational region in this study.

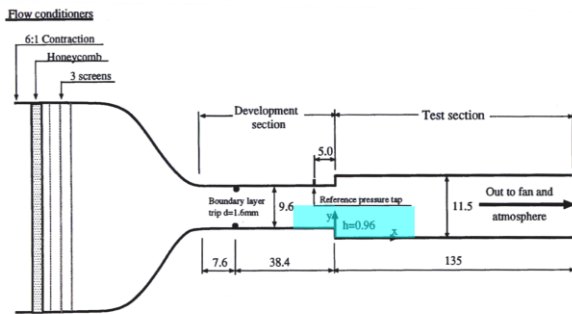


Fig. 3. Backward-facing step configuration [16]

The synthetic jet is located near the edge of backward facing step because previous study [3] presents synthetic jet location near the separation point (the edge of backward facing step) is favorable. The cavity of synthetic jet is located between $-0.5h$ and $0.125h$ from edge of backward facing step. (See Fig.6)

C. Flow conditions

Inlet flow Mach number and Reynolds number based on height of backward-facing step and freestream velocity are 0.2 and 5000, respectively. 99 percent boundary layer thickness is $1.2h$ at $x/h = -3.15$. Inflow boundary layer is turbulent. Reynolds number and boundary layer thickness are the same as those of Jovic's study [17]. Synthetic jet has two important input parameters that are commonly used to describe the operating conditions for flow control; non-dimensional frequency and momentum coefficient. Non-dimensional frequency denotes the frequency of the wall oscillation of synthetic jet and non-dimensional momentum coefficient denotes ratio of momentum of synthetic jet and free stream.

$$F_h^+ = fh / u_\infty \quad C_\mu = \rho u_j^2 d / \rho u_\infty^2 h \quad (2)$$

where f , h , u_∞ , ρ , u_j , and d are the dimensional frequency of the wall oscillation, height of backward-facing step, freestream velocity, density and averaged maximum velocity at orifice exit. The present analysis is focused on the frequency characteristics of the synthetic jet. Three cases are selected, Synthetic-jet-off (without synthetic jet), $F_h^+ = 0.2$ and $F_h^+ = 2.0$, where non-dimensional frequency F_h^+ is normalized with height of backward-facing step and freestream velocity. Previous studies around airfoil [3-5] showed that both these values are good for control, respectively. In this study, momentum coefficient is set to the same value (0.2 percent) for each case since the present analysis is focused on the frequency characteristics of the synthetic jet. The value of momentum coefficient is very small compared with that of blowing jet which successfully controls separation. The amplitude use different value of $F_h^+ = 0.2$ and $F_h^+ = 2.0$ because u_j is proportional amplitude and frequency as shown equation (3). (See Table 2)

$$u_j = k \cdot A \cdot F_h^+ \quad (3)$$

Table 1. Computational conditions

F_h^+	C_μ	Amp.
0.2	0.20%	0.041
2	0.20%	0.0041

COMPUTATIONAL METHODS

A. Numerical method

Three-dimensional compressible Navier-Stokes equations nondimensionalized by freestream sound speed, density, and reference length are employed as the governing equations. These equations are solved in the generalized curvilinear

coordinates. The spatial derivatives of convective terms and viscous terms, metrics, and Jacobian are evaluated by the sixth-order compact difference scheme [8] since an induced velocity by synthetic jet is very small and the boundary layer is efficiently solved. Near the boundary, second-order explicit difference schemes are used. The tenth-order filtering [9] is used with filtering coefficient of 0.45. Visbal and Gordnier's approach [10] for computation of metrics and Jacobian on deforming and moving meshes is used for satisfying the geometric conservation law. For time integration, regarding the characteristic of the computer, a kind of implicit method alternating direction implicit and symmetric Gauss-Seidel (ADI-SGS) is used for time integration. This algorithm uses same kind of idea of four-factored symmetric Gauss-Seidel (FF-SGS) [11] which adopt both ideas of the lower-upper symmetric alternating direction implicit (LU-ADI) and the lower-upper symmetric Gauss-Seidel (LU-SGS). To ensure the time accuracy, backward second-order difference formula is used for time integration whereas three sub-iterations [12] are adopted. The computational time step is 0.003 in non-dimensional time so that the maximum Courant-Friedrichs-Lewy (CFL) number becomes approximately 2.0. In the standard LES approach, explicit subgrid scale model are employed, but in ILES approach [13] they are not employed. Instead, a high-order low-pass filter selectively damps poorly resolved high-frequency waves. Direct numerical simulation (DNS) is not used because the present computational resources are not sufficient for DNS, and the analysis of vortex structure that can be resolved using LES is sufficient for understanding the flow control mechanism. Turbulent inflow boundary conditions are generated by using rescaling method of Urbin *et al.* [14]. Rescaling domain is $-12.0 < x/h < -2.0$. Outflow boundaries are located away from the edge of backward facing step by rapid stretching the mesh in the streamwise direction [15]. At the outflow boundary, all variables are extrapolated. On the lower surface, no-slip conditions are adopted along with a zero normal pressure gradient. Finally, the upper surface is treated as a slip wall ($W = 0$) and the normal derivative of other variables is set to zero. Periodic boundary condition is applied to the spanwise direction.

B. Computational grids

Fig. 4 shows side-view of backward-facing step. A computational region is aqua region near edge of backward-facing step as shown in Fig.3. The length of the computational region of zone1 in streamwise direction (x -direction) is $12h$ because the rescaling domain is $-12.0 < x/h < -2.0$. Fig. 5 shows top view of backward-facing step. The length of the computational region in span direction (y -direction) is $4h$. A

buffer region is configured [15] to avoid non-physical reflection of acoustic wave as shown in Fig. 4 and Fig. 5. The orifice and cavity configuration of synthetic jet is two-dimensional configuration as shown in Fig. 7. Patched grids approach [18] is employed to generate grids for cavity, orifice, and backward-facing step regions, as shown in Fig. 6 and 7. Synthetic-jet-off case does not include cavity and orifice region. The grid deformation approach developed by Melville *et al.* [19] is applied to generate a time-varying fluid grid system for the cavity region as shown in Fig. 6 and 7. This algebraic method can maintain the grid quality of the initial grid near the deforming surfaces under arbitrary, moderate deflections and rotations. The total number of the grid points is about 7,000,000. (See Table. 1) Note that the spatial resolution of a sixth-order compact difference scheme is, in general, much finer than a conventional low-order upwind scheme. Our experience indicates that the results with the present method would correspond to those from a conventional scheme with 50 to 100 times more grid points. Between each region, 12 grid points are overlapped to maintain the same accuracy as the internal grid points in overlapped region. The minimum grid size in each direction of all grids is $dx = 0.0017$, $dy = 0.04$ and $dz = 0.0017$, respectively. (Δx^+ , Δy^+ , Δz^+_{\min}) are (4, 5, 0.2) in zone 1, respectively, these value is sufficient for resolving turbulent boundary layer. The grid points, minimum grid spacing and computational region are referenced by Huang *et al.* [18]. A grid sensitivity study is performed as preliminary study.

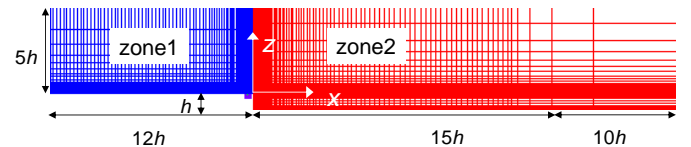


Fig. 4. Computational region (side-view)

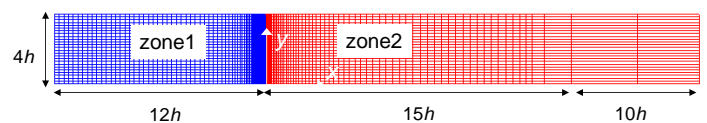


Fig. 5. Computational grid (top-view)

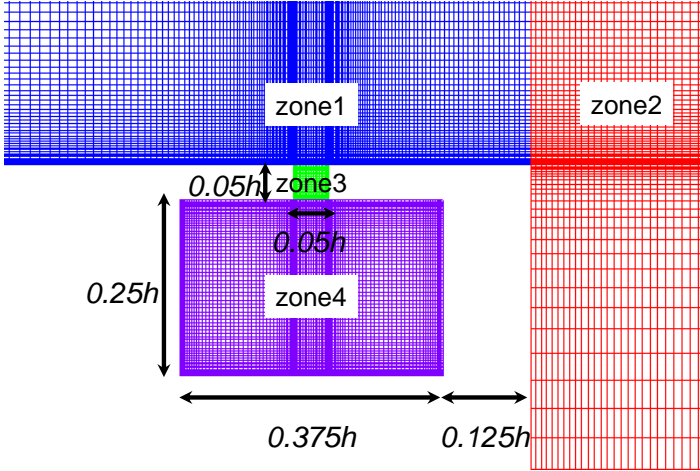


Fig. 6. Computational grid (side-view of synthetic jet)

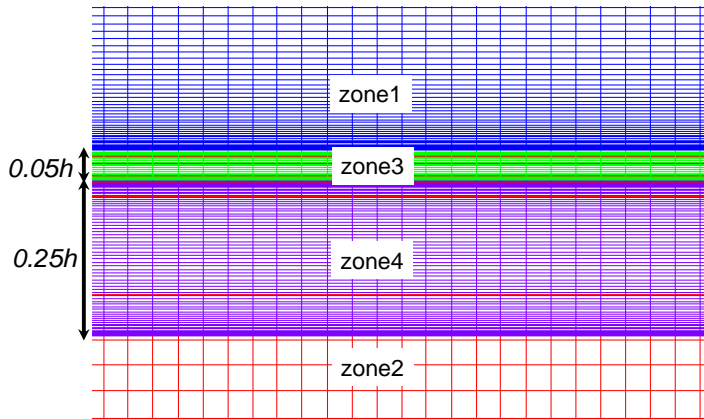


Fig. 7. Computational grid (front view of synthetic jet)

Table 2. Grid points

zone	name	$j \times k \times l$	$\Delta x/h$	$\Delta y/h$	$\Delta z/h$
zone1	Backstep	349×101× 85	0.0017	0.04	0.0017
zone2	Backstep	268×101×138	0.0027	0.04	0.0017
zone3	orifice	21×101× 43	0.0017	0.04	0.0017
zone4	cavity	99×101× 65	0.0017	0.04	0.0017

RESULTS AND DISCUSSION

Validation

Validation are shown in our previous paper[21]. The numerical errors included in the present computations are sufficiently small for understanding the frequency and amplitude characteristics of the synthetic jet and flow field.

Time averaged flow-fields

Figure 8 shows skin friction coefficient on the bottom wall ($0.0 < x/h < 10.0$) for each cases. Reattachment length of $F_h^+ = 0.2$ is obviously shorter than Synthetic-jet-off and $F_h^+ = 2.0$. Table 3 presents reattachment length computed from skin friction coefficient and shows that length of separation region of $F_h^+ = 0.2$ is 20 percent shorter than the Synthetic-jet-off case. Figure 9 shows Reynolds stress distribution for each case. At the Synthetic-jet-off case, strong Reynolds stress regions exist from the shear layer region ($0.0 < x/h < 2.0$) and the recirculation region ($2.0 < x/h < 6.0$). High Reynolds stress distribution enhances mixing of shear layer, and separated flow reattach in the case of $F_h^+ = 0.2$. The Reynolds stress distribution of $F_h^+ = 2.0$ is almost the same as that of the Synthetic-jet-off case. The shear layer flow-directional evolution can be analyzed by computing the vorticity and momentum thickness. Figure 10 shows the vorticity thickness of shear layer. The vorticity thickness is usually used as reference value of thickness scale of mixing layer and shear layer. The vorticity thickness of $F_h^+ = 0.2$ case is totally larger than those of the others. The Reynolds stress distribution increases at $x/h = 1.5$ (Fig. 9). On the other hand, at $F_h^+ = 2.0$, the vorticity thickness is almost the same as synthetic-jet-off case and slightly smaller at the recirculation region ($4.0 < x/h < 6.0$). Figure 11 shows the momentum thickness of shear layer. The momentum thickness is used as reference value of mixing. The momentum thickness of $F_h^+ = 0.2$ case is large. On the other hand, at $F_h^+ = 2.0$, the momentum thickness is almost the same as Synthetic-jet-off case and slightly smaller at the recirculation region ($4.0 < x/h < 6.0$). These time-averaged flow-fields illustrate that the Reynolds stress, shear layer thickness, mixing and reattachment point have strong correlation and the Reynolds stress seems to be important index of reattachment point.

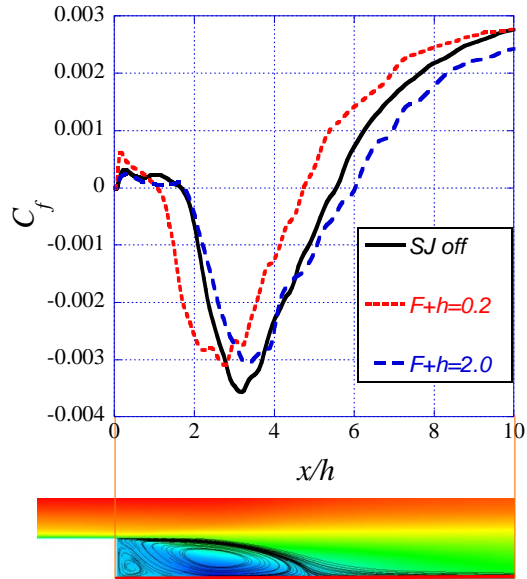


Fig.8. Skin frictional Coefficient

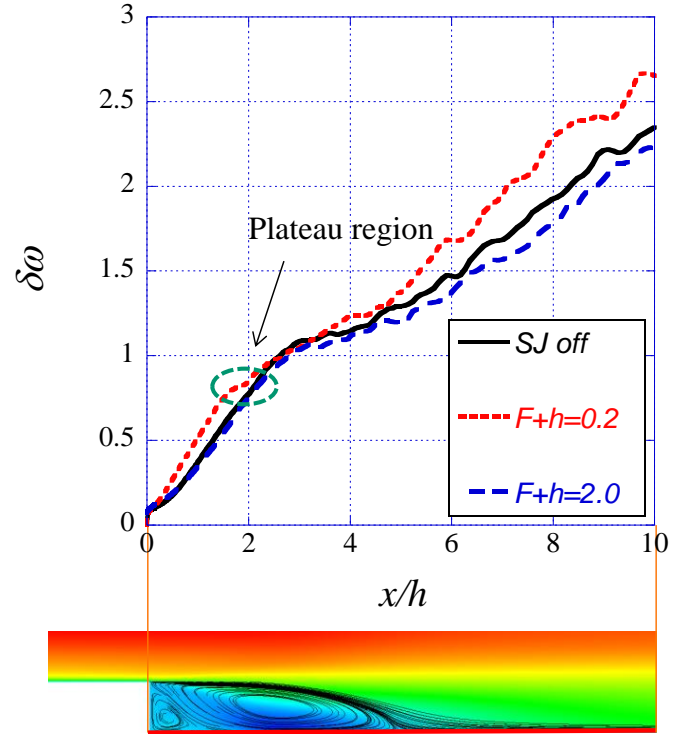


Fig.10. Vorticity thickness evolution along shear layer

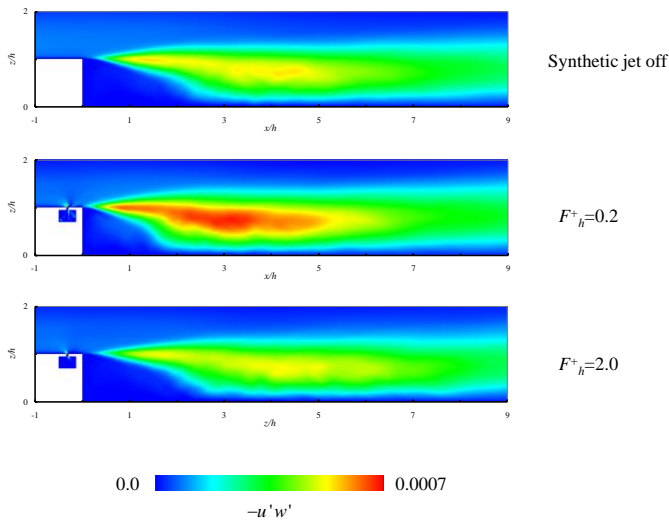


Fig. 9. Reynolds stress distribution

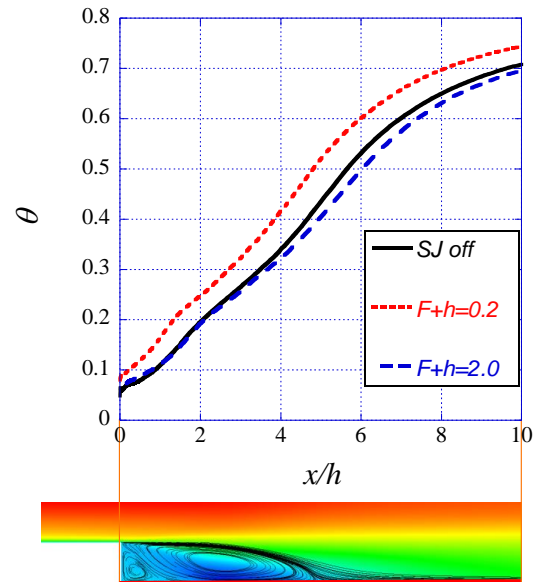


Fig. 11. Momentum thickness evolution along shear layer

Table 3 Reattached location

	Reattainment location
synthetic jet off	$5.85h$
$F_h^+ = 2.0$	$6.0h$
$F_h^+ = 0.2$	$4.75h$

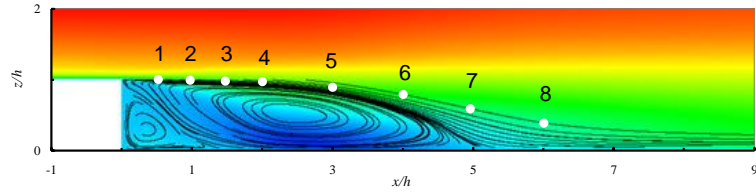


Fig. 12. Location of spectrum measured points

Spectral analysis

Spectral analysis is conducted and frequency characteristics of flow-field are quantitatively investigated, Figure 12 presents the location of spectrum measured points from station 1 to 8. These locations are along the time averaged shear layer of synthetic-jet-off case. The spectra are averaged 10 points with spanwise direction for each. Figure 13, 14 and 15 show one-third octave band filtered power spectrum densities of vertical velocity at synthetic-jet-off, $F_h^+ = 0.2$ and 2.0 , respectively. Power spectrum densities are filtered by one-third octave band and noises on spectrum data are cleaned up. The vertical velocity is chosen as observed value because the vertical velocity shows clearer frequency characteristics of the shear layer and the vortices than pressure and density. In synthetic-jet-off case, the station 1 has peak at $St=0.4$ and peak value is smaller than other stations. The station 2 has peak at $St=0.2$ and peak value is sufficiently high. With stations moving to downstream region, the peak move to low frequency side and peak value increases because shear layer develops as shown in Figs. 10 and 11. This corresponds to that the vortex scale is increasing at downstream region (the details are described in next section). All the cases have this trend, more or less. In $F_h^+ = 0.2$ case, the station 1 has three clear peaks at $St=0.2, 0.4$ and 0.6 and first and second peak value is dominant. The first peak corresponds to vortices generated from the synthetic jet, while the second and third peaks corresponds vortices induced from the shear layer. The vortices of various scales are generated in the shear layer. At the station 5 ($x/h=1.5$), peak values of second ($St=0.4$) and third ($St=0.6$) peaks decrease because of vortex pairing. This observation corresponds to the vorticity thickness reaches a plateau as shown in Fig. 10. Ho and Huang[22] also show the start of the plateau agree the location of vortex merging. At the station 7, first peak ($St=0.2$) disappears because the vortices break. Additionally, the start and end locations of strong Reynolds stress region agree well with location of vortex merging and diffusing as shown in Fig. 10. In $F_h^+ = 2.0$ case, the station 1 has the peak corresponding to actuation. This shows that vortices generated by actuation of synthetic jet at $St=2.0$. The level of the spectra at high frequency region of this case is higher than that of the other cases because synthetic jet is actuated at high frequency ($F_h^+ = 2.0$). The whole tendencies of spectrum are almost the same as Synthetic-jet-off case except for high frequency region.

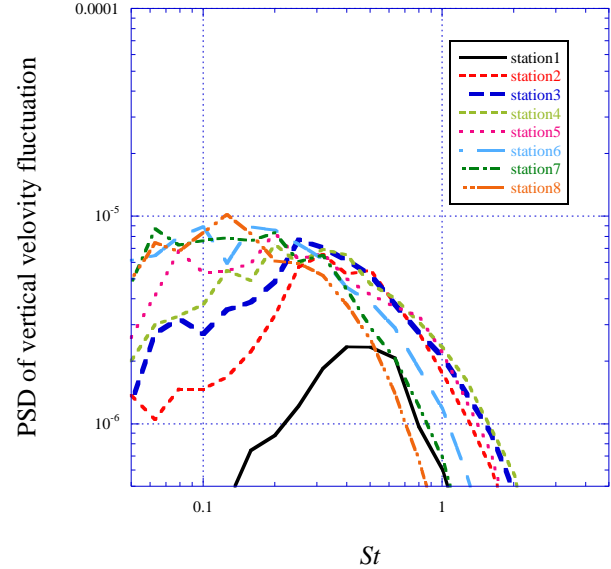


Fig. 13. One-third octave band filtered Power Spectrum Density of vertical velocity fluctuation, (Synthetic jet off)

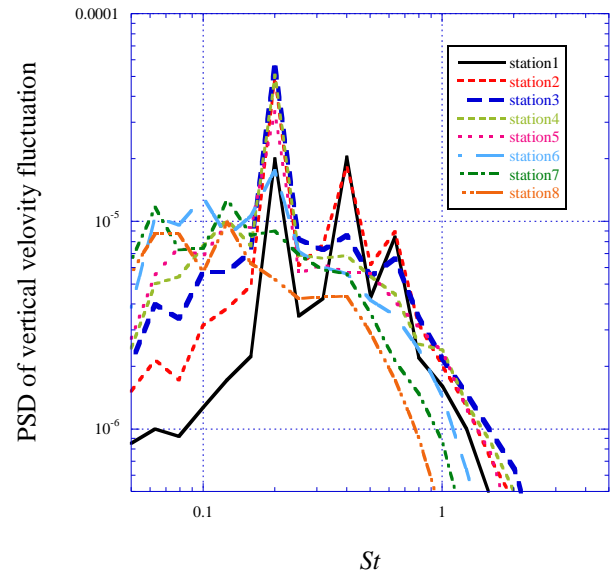


Fig. 14. One-third octave band filtered Power Spectrum Density of vertical velocity fluctuation, ($F_h^+ = 0.2$)

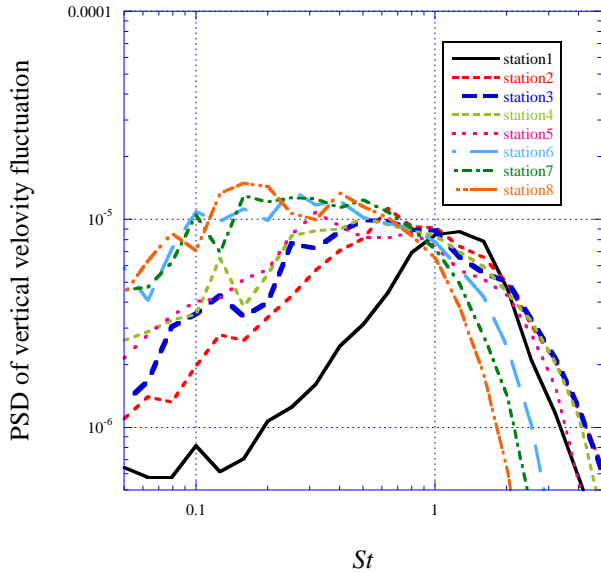


Fig. 15. One-third octave band filtered Power Spectrum Density of vertical velocity fluctuation, ($F+h=2.0$)

Phase-averaged analysis

Phase averaged analysis is conducted and the generation mechanism of Reynolds stress in $F^+_h=0.2$ case is investigated. Phase average analysis is effective methods for periodical phenomenon or turbulent shear layer and mixing layer. Phased averaged distinguish the periodic fluid motion and turbulent one. The frequency of phase averaging is set to the same as the synthetic jet actuation. This frequency is most dominant as shown in Fig. 14. Figure 16 presents phase-and-span-averaged static pressure and second invariant of the velocity gradient tensor Q at each phase. The vortices are developing near the edge of backward-facing step and vortex diffuses at the down-stream. At $\phi=1/4\pi$, the vortex generated from synthetic jet and vortices induced from the edge of backward-facing step are pairing. At $\phi=6/4\pi$, Second pairing occurs at $x/h=1.5$ as shown in spectrum analysis (Fig. 14). Figure 17 shows periodic and turbulent component of Reynolds shear stress distribution. The time and span averaged Reynolds shear stress can divide periodic and turbulent components using phase averaged analysis. The periodic component is dominant near the backward-facing step, while turbulent component is totally dominant and especially strong from $x/h=1.5$ to 5.0 . Figure 18 shows periodic and turbulent components of Reynolds shear stress distribution and Second invariant of the velocity gradient tensor Q at the each phase. The developing vortices induce the periodic component from $x/h=0.0$ to $1.5h$. The turbulent component is induced between vortices and vortices. To investigate the mechanism of Reynolds stress of turbulent component, phase averaged (not span averaged) isosurfaces Q are shown in Fig.19 and 20. Isosurfaces in Fig. 19 are colored by x -vorticities ω_x . Two-dimensional coherent

vortices (roller) and longitudinal vortices (rib or braid) are visualized by phased average analysis. The longitudinal vortices are observed between the two-dimensional vortices. Isosurfaces in Fig. 20 are colored by Reynolds shear stress of turbulent component. The region of strong Reynolds stress corresponds to the region where strong x -vortices are observed. These results show that x -vortices stretching generate turbulent component of Reynolds shear stress. These vortex structure and generation mechanics of Reynolds stress of turbulent component correspond to those in the turbulent mixing layer.

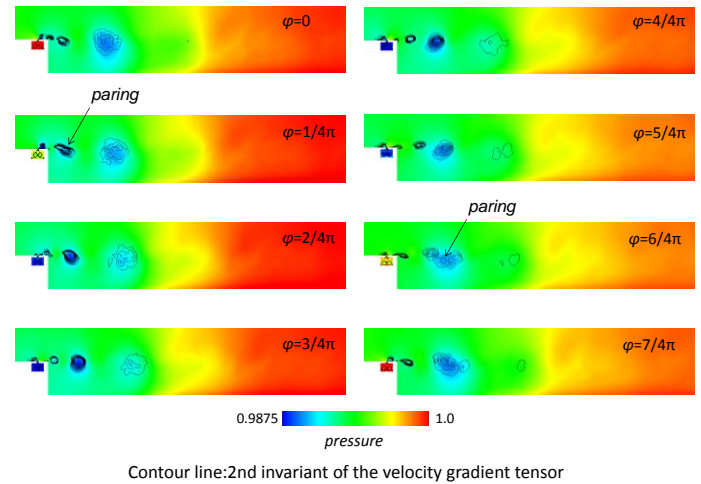


Fig. 16. Phase and span averaged static pressure and Second invariant of the velocity gradient tensor (black lines, contour range:0.05-0.5 with 10 lines)

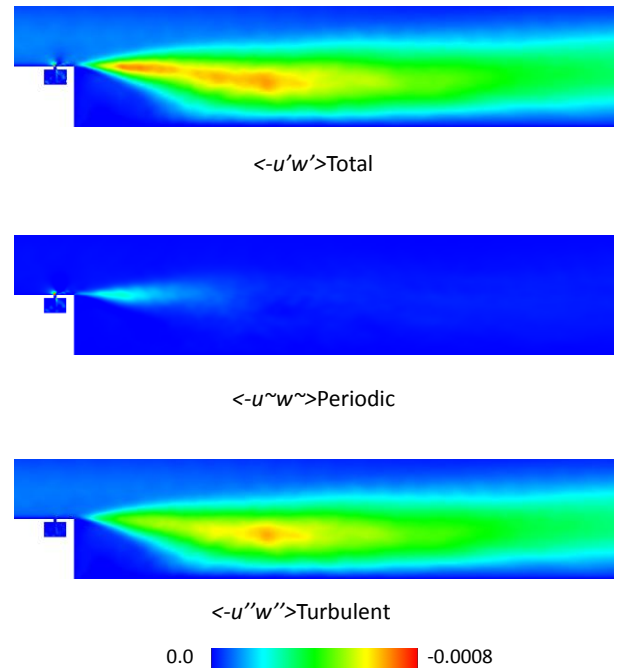


Fig. 17. Phase and span averaged Total component, periodical component and turbulent component of

Reynolds shear stress distributions

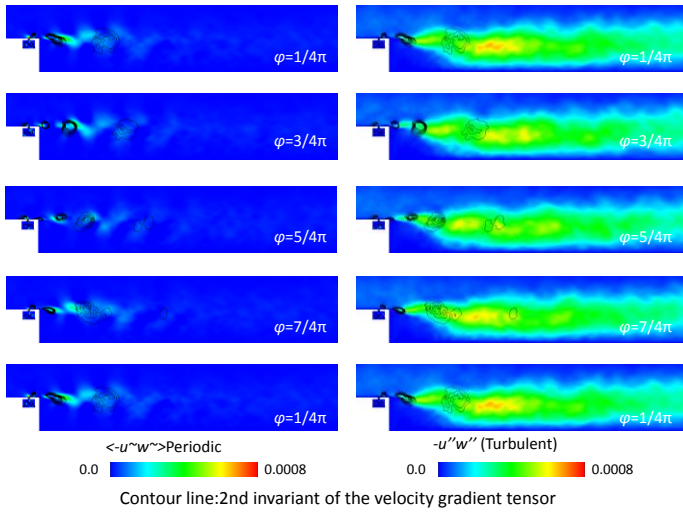


Fig. 18. Phase and span averaged periodical component and turbulent component of Reynolds shear stress distributions and Second invariant of the velocity gradient tensor at the each phase (black lines, contour range: 0.05-0.5 with 10 lines)

Longitudinal vortices (rib)

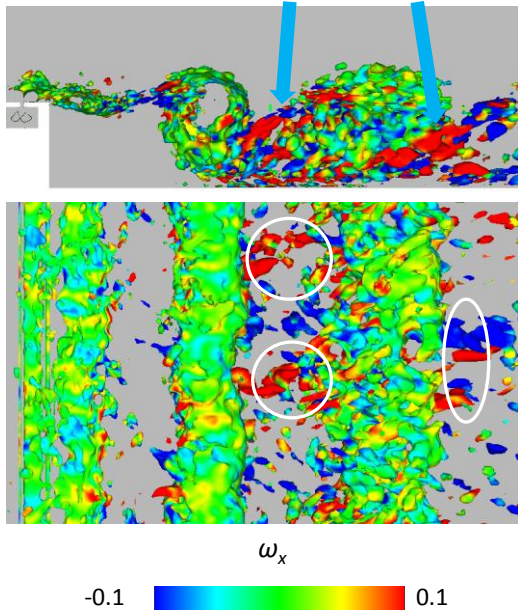


Fig. 19. isosurfaces of Second invariant of the velocity gradient tensor (isosurface is colored by x-vorticity)

Strong Reynolds stress

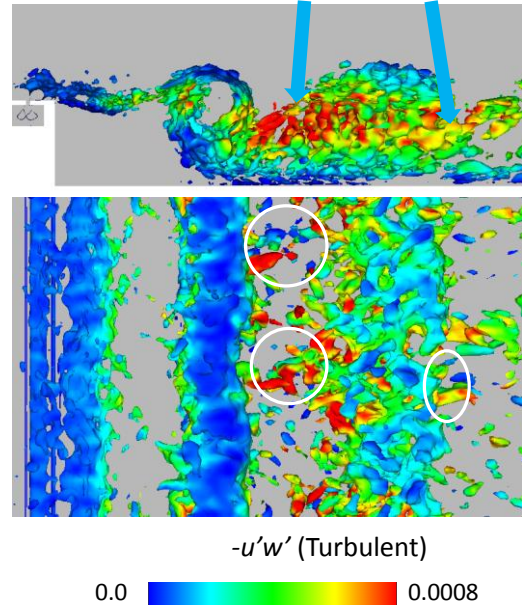


Fig. 20. isosurfaces of Second invariant of the velocity gradient tensor (isosurface is colored by turbulent component of Reynolds shear stress)

SUMMARY

The present computation shows that at $F_h^+ = 0.2$, length of separation region is 20 percent shorter than the synthetic jet off case. Strong two-dimensional vortices induced from the synthetic jet interact and merge with the shear layer, which results in the increase of the periodic component of Reynolds stress in the shear layer region. The longitudinal vortices induced by pairing two-dimensional vortices, which make the turbulent component of Reynolds stress stronger in the recirculation region. At $F_h^+ = 2.0$, length of the separation region is almost the same as the synthetic jet off case because mixing is not enhanced in the shear layer and recirculation region. Weak and short periodic vortices induced from the synthetic jet do not interact with the shear layer very much and diffuse in the recirculation region.

REFERENCES

[1] Okada, S. and Hiraoka, K. (2003), "Experimental Studies of Reduction of the Wing Tip Vortex by Suction," AIAA Paper 2003-3533.
 [2] Mallinson, H. (1999), "Some Characteristics of Synthetic Jets," AIAA Paper 99-3651.
 [3] Amitay, M. et al. (2001), "Aerodynamic flow control over an unconventional airfoil using synthetic jet actuators," AIAA Journal, Vol.39, 356-370.

- [4]Seifert, A. and Darabi, A. (1996), "Delay of Airfoil Stall by Periodic Excitation," *Journal of Aircraft*, Vol. 33, 691-699.
- [5]Glezer A., Amitay, M. et al. (2005), "Aspect of Low-and High-Frequency Actuation for Aerodynamic Flow Control," *AIAA Journal*, Vol.43, 1501-1511.
- [6]Yoshioka, S., Obi, S. and Masuda, S. (2001), "Turbulence Statistics of periodically perturbed separated flow over backward-facing step," *International Journal of Heat and Fluid Flow*, vol. 22, 393-401.
- [7]Okada, K.; Oyama, A.; Fujii, K. and Miyaji, K. (2010), 'Computational Study on Effect of Synthetic Jet Design Parameters', *International Journal of Aerospace Engineering*.
- [8]Lele, S.K. (1992), "Compact Finite Difference Scheme with Spectral-Like Resolution," *Journal of Computational Physics*, Vol.103, 16-22.
- [9]Gaitonde, D.V. and Visbal, R.M. (2000), "Pade Type Higher-Order Boundary Filters for the Navier-Stokes Equations," *AIAA Journal*, Vol.38, No.11, 2103-2112.
- [10]Visbal, R.M. and Gordnier, R.E. (2000), "Higher-Order Flow Solver for Deforming and Moving Meshes," *AIAA Paper 2000-2619*.
- [11]Fujii, K. (1999), "Efficiency Improvement of Unified Implicit Relaxation/Time Integration Algorithms," *AIAA Journal*, Vol. 37, No. 1, 125-128.
- [12]Chakravarthy, S. R. (1984), "Relaxation Methods for Unfactored Implicit Upwind Schemes," *AIAA Paper 84-0165*.
- [13]M. R. Visbal, and D. P. Rizzetta (2002), "Large-eddy simulation on general geometries using compact differencing and filtering schemes," *AIAA Paper 2002-288*.
- [14]Gerald Urbin and Doyle Knight, (2001) "Large-Eddy Simulation of a Supersonic Boundary Layer Using an Unstructured Grid," *AIAA Journal* vol.39 No.7, 1288-1295.
- [15]T. Colonius, S. K. Lele and P. Moin (1993), "Boundary Condition for Direct Computation of Aerodynamics Sound Generation," *AIAA Journal*, vol. 31, No. 9.
- [16]Rizzetta, D. and Visbal, R.M. (1999), "Numerical Investigation of Synthetic Jet Flowfields," *AIAA Journal*, Vol.37, No.9, 919-927.
- [17]Srba Jovic (1994), "Backward-Facing Step Measurements at Low Reynolds Number, $Re_h=5000$," *NASA TM -08807*
- [18]Fujii, K. (1995), "Unified Zonal Method Based on the Fortifies Solution Algorithm," *Journal of Computational Physics*, Vol.118, 92-108.
- [19]Melville R. B., Morton S. A. and Rizzetta D. P. (1997), "Implementation of a Fully-Implicit, Aeroelastic Navier-Stokes Solver," *AIAA Paper 97-2039*.
- [20]Hung Le, Parviz Moin and John Kim (1997), "Direct numerical simulation of turbulent flow over a backward-facing step" *Journal of Fluid Mechanics*, Vol. 330, pp.349-374.
- [21]Okada K, Fuji K., Miyaji K(2009), "Computational Study of Frequency and Amplitude Effects on Separation Flow Control with the Synthetic Jet" *ASME/IMECE2009, IMECE2009-11218*
- [22]Ho, C. M. and Huang, L. S. (2002), "Subharmonics and vortex merging in mixing layers," *Journal of Fluid Mechanics*, Vol. 119, pp. 443- 473.